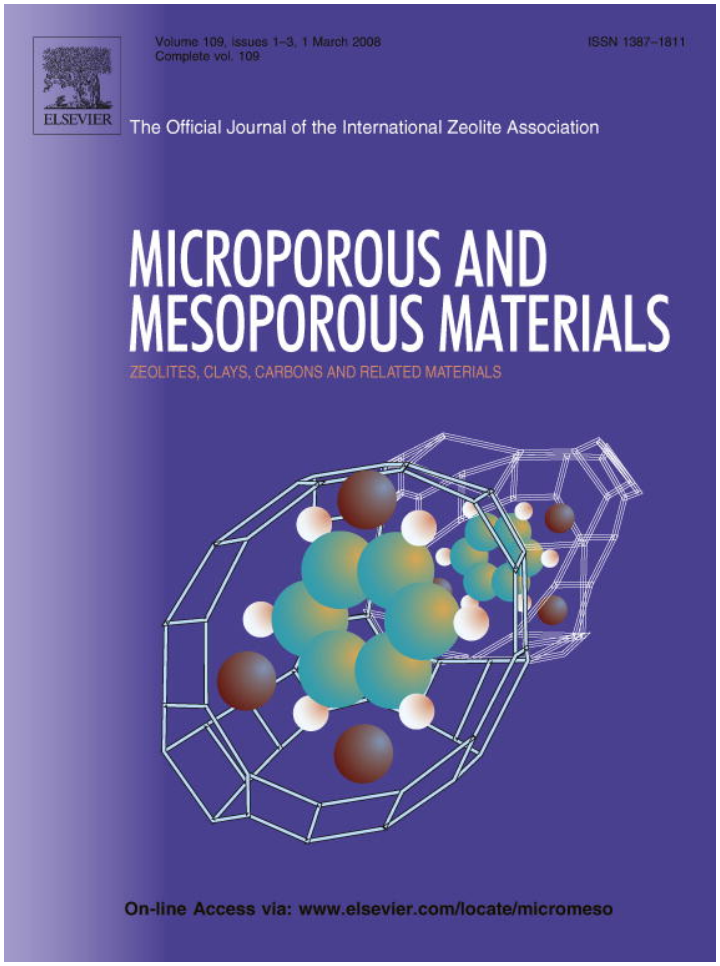

Available online at www.sciencedirect.com
ScienceDirect
Microporous and Mesoporous Materials 109 (2008) 505–512
MICROPOROUS AND MESOPOROUS MATERIALS
www.elsevier.com/locate/micromeso

Nickel hexacyanoferrate multilayers on functionalized mesoporous silica supports for selective sorption and sensing of cesium

Chin-Yuan Chang, Lai-Kwan Chau *, Wei-Ping Hu, Chiou-Yann Wang, Ju-Hsiou Liao

Department of Chemistry and Biochemistry National Chung Cheng University, 168 University Road, Min-Hsiung, Chia-Yi 621, Taiwan, ROC

Received 5 July 2006; received in revised form 25 May 2007; accepted 30 May 2007
Available online 13 June 2007

Abstract

The preparation and characterization of a novel material, multilayers of nickel hexacyanoferrate immobilized on mesoporous propylethylenediamine triacetate functionalized silica supports, and its uses as a cesium sorbent and a cesium sensing material is reported. The preparation of nickel hexacyanoferrate multilayers is based on multiple sequential adsorption of Ni^{2+} and $Fe(CN)_6^{4-}$. This material was evaluated for selective removal of cesium ions in the presence of competing metal ions from water. Loading capacity of at least 2.25 mg (1.69 mmol) per gram of sorbent material has been achieved, making it potentially useful for the removal of cesium from nuclear wastes and contaminated groundwater. This material was also coated on a glassy carbon electrode for voltammetric sensing of cesium ions. The Nernst plot for the film has a linear range between 10^{-6} and 1 M and a slope of 31 mV/decade. The material was characterized through infrared spectroscopy, nitrogen adsorption, X-ray powder diffraction, cyclic voltammetry, and the Ni and Fe precursors and a reaction complex were modeled computationally by the PM3™ semiempirical method.

Keywords: Nickel hexacyanoferrate; Organically modified sol–gel silica; Sorbent; Chemical sensor; Cesium

1. Introduction

Radioactive cesium contamination of water is of serious social and environmental concern since it is a significant fraction of the radioactivity of the liquid waste from the reprocessing of nuclear fuel [1]. Nickel hexacyanoferrate (NiHCF) has been widely studied for separation [2,3] and electrochemical sensing [4,5] of Cs^+ owing to its strong selectivity for Cs^+ over other radionuclides and alkali cations [6–8] and its high Cs^+ sorption capacity over many metal hexacyanoferrates (MHCFs) [9]. Furthermore, its ion uptake and elution can be controlled directly by modulating the potential of the electroactive NiHCF film [10]. This characteristic has potential implications for the monitoring and remediation of aqueous phase nuclear wastes containing $^{137}Cs^+$.

So far, NiHCF products prepared by precipitation methods are usually in very fine powders which are difficult to be separated from aqueous solution by filtration and have too low a permeability for column work [2]. Thin films of NiHCF have been deposited by either chemical [11] or electrochemical methods [12–14]. Films from chemical deposition are usually not robust, whereas films from electrochemical deposition are only allowed on conductive or semiconductive substrates. Thus, aspects such as sorption capacity, toughness, cracklessness, and high adherence to various surfaces, have to be considered in the deposition of NiHCF films. To overcome the adhesion problem, functionalized surfaces have been used to anchor a MHCF monolayer or film on those surfaces [15,16].

Recently, a new branch of research has evolved on the synthesis of nanoporous materials. Through the marriage of nanoporous silica materials with self-assembled monolayer chemistry, a powerful new class of sorbent materials functionalized with a monolayer of MHCF has been designed for remediation of cesium contamination [17,18].

* Corresponding author. Tel.: +886 5 2720411x66411; fax: +886 5 2721040.
E-mail address: chelkc@ccu.edu.tw (L.-K. Chau).

1387-1811/$ - see front matter © 2007 Elsevier Inc. All rights reserved.
doi:10.1016/j.micromeso.2007.05.057

Nevertheless, an even higher sorption capacity is expected if a self-assembled multilayer system can be formed on the surfaces of such nanoporous materials. Among the self-assembled multilayer systems, multilayers formed by the interaction between the ionic constituents using alternate adsorption of cations and anions are of particular interest as they are easy to prepare and have good stability [19–21]. We reasoned that a similar chemistry could be used to self-assemble NiHCF in a nanoporous structure.

In this paper, we describe a simple method to produce NiHCF multilayer based on multiple sequential adsorption of Ni^{2+} and $Fe(CN)_6^{4-}$ on a porous organically modified silica (OMS) material formed by the sol–gel process. The OMS material, named propyl-ethylenediamine triacetate functionaliezd silica (PEDTAFS), incorporates an organic substituent, propyl-ethylenediamine triacetate (PEDTA) [22], which chelates Ni(II) and acts as an anchoring site for the NiHCF multilayer to grow. Such a nanocomposite was characterized by infrared spectroscopy, nitrogen adsorption, energy dispersive X-ray spectroscopy, powder X-ray diffraction, cyclic voltammetry, and the structure of Ni and Fe precursors and the reaction complex of the initial step in the formation of NiHCF were modeled computationally. Its uses as a cesium sensor and as a high loading sorbent material for cesium binding have also been demonstrated.

2. Experimental

2.1. Materials

The following chemicals were used in the synthesis of sol–gel-derived materials: tetramethyl orthosilicate (TMOS, Tokyo Chemical Industry), *N*-(trimethoxysilylpropyl)ethylenediamine triacetic acid, trisodium salt (TMSPEDTA, 50% w/w Gelest), and hydrochloric acid (Merck). Potassium ferrocyanide (Fisher Scientific), nickel nitrate hexahydrate (Showa), cesium nitrate (NOAH), potassium nitrate (Osaka), sodium nitrate (Showa), and sodium dichromate (Hanawa) was used as received without further purification. All aqueous solutions were prepared with water that had been purified by using a Milli-Q water purification system (Millipore) with a specific resistance of 18 MΩ cm.

2.2. Preparation of NiHCF-modified electrode

Glassy carbon (GC) electrodes (diameter 3 mm, Bioanalytical Systems) were polished with 0.05 μm alumina powder on a napless polishing cloth and sequentially cleaned with acetone, methanol, and water in an ultrasonic bath for 30 min in each step. Subsequently, the GC electrodes were electrochemically oxidized in 10% HNO_3 + 2.5% $K_2Cr_2O_7$ at 2.2 V versus Ag/AgCl for 10 s. The electrodes were then soaked in TMSPEDTA for one hour, air-dried in a closed container for 24 h, and stored in water before further modification. To prepare the NiHCF films, the TMSPEDTA-modified electrodes were placed alternatively in a 10 mM $Ni(NO_3)_2$ solution and a 10 mM $K_4[Fe(CN)_6]$ solution for 5 min each. At each stage of modification, the surface is rinsed thoroughly with water to remove any physically adsorbed Ni^{2+} or $Fe(CN)_6^{2-}$. The above deposition cycle was repeated to obtain the desirable number of NiHCF layers.

2.3. Preparation of NiHCF–PEDTAFS powder

PEDTAFS powder and TMOS-derived powder were prepared as described previously [22]. NiHCF was immobilized on the PEDTAFS powder by first immersing the powder in a solution of 10 mM $Ni(NO_3)_2$ for 5 min. The Ni(II)-treated powder was then filtered through a 6 μm micron filter and rinsed with water. Subsequently, the filtered powder was immersed in a solution of 10 mM $K_4[Fe(CN)_6]$ for 5 min. After the ferrocyanide treatment, the powder was filtered through a 6 μm micron filter and rinsed with water. The above steps were then repeated five times.

2.4. Cesium sorption studies

Exactly 0.1 g NiHCF–PEDTAFS powder or PEDTAFS powder was added to 100 mL of a cesium ion solution for 60 min. The treated powder was then filtered through a 6 μm micron filter and rinsed with water until cesium in the filtrate was not detectable. The detection of cesium was performed by flame atomic emission spectroscopy (AES), which showed an emission band at 852.1 nm if cesium was present. The amount of cesium sorption by NiHCF–PEDTAFS powder or PEDTAFS powder was taken as the difference between the initial Cs concentration and the residual Cs concentration. In cases where the samples contain a competing ion such as sodium or potassium, the above cesium sorption procedures also applied.

2.5. Instrumentation

The PEDTAFS gels were lyophilized to powder by a Kingmech FD-2-12P freeze dryer. Infrared absorption spectra were measured with a Jasco FT-IR spectrometer by dispersing the NiHCF–PEDTAFS or PEDTAFS powder in KBr and pressed into pellet form. The pore structure was studied by N_2 adsorption isotherms (at 77 K) of the samples, previously outgassed for 6 h at 393 K, using an ASAP 2020 Surface Area and Porosimetry System by Micrometrics. Energy dispersive X-ray (EDX) spectra were obtained with a Jeol JSM-6500 F scanning electron microscope. X-ray powder diffraction (XRPD) measurements were performed on a Shimadzu XRD-6000 diffractometer equipped with Ni-filtered CuKα radiation. Simulated XRPD patterns for bulk NiHCF were generated by the software Crystallographica (Oxford Cryoststems), based on the single-crystal data obtained from Inorganic Crystal Structure Database (FIZ Karlsruhe). Cyclic voltammograms were recorded with an electrochemical analyzer (Model 421, CH Instruments).

A one-compartment three-electrode cell with an Ag/AgCl reference electrode (3 M NaCl, Bioanalytical Systems) and a platinum counter-electrode was employed. All potentials reported here are referred to the Ag/AgCl reference electrode (3 M NaCl). Concentration of cesium was measured by a Perkin–Elmer 3100 atomic absorption/emission spectrophotometer. The theoretical modeling of the Ni and Fe precursors and the initial reaction complex were performed using the PM3™ semiempirical method in the Hyperchem pro 6.0 program [23].

3. Results and discussion

3.1. Synthesis and characterization of NiHCF–PEDTAFS

Films of MHCF from direct chemical deposition on unmodified surfaces are usually not robust. The PEDTA group has been shown to chelate with a number of transition metal cations [22], making it very useful as a foundation upon which to build a variety of different MHCF films. Fig. 1 shows the IR spectra of PEDTAFS and NiHCF–PEDTAFS powder. Several absorption bands evident in Fig. 1a represent antisymmetric carboxylate stretching vibration $\nu_a(CO_2^-)$ at 1624 cm^{-1} and vibrations of Si–O–Si bonds at 1075 cm^{-1}. The band near 1416 cm^{-1} is due to a strong coupling between the symmetric carboxylate stretching vibration $\nu_s(CO_2^-)$ and the methylene bending vibration of the α-CH_2 group [24]. It is well-known that frequencies for carboxylate are variable and depend on counter cations [25–27]. As shown in Fig. 1b, the shift of $\nu_a(CO_2^-)$ in NiHCF–PEDTAFS to 1595 cm^{-1} indicates that Ni^{2+} likely interacts with the carboxylates in NiHCF–PEDTAFS. Also shown in Fig. 1b, a new band at 2050 cm^{-1} appears. This intense band is characteristic of a bridging cyanide ligand, not a terminal species, offering direct evidence that the bridged dinuclear [Ni, Fe] species [7,18,28–30] is successfully immobilized on the PEDTA-functionalized silica surface. The relatively low frequency of the CN stretching mode also indicates that the bridging cyanide ligand is in the vicinity of Fe(II) [7]. The porous NiHCF–PEDTAFS powder had a

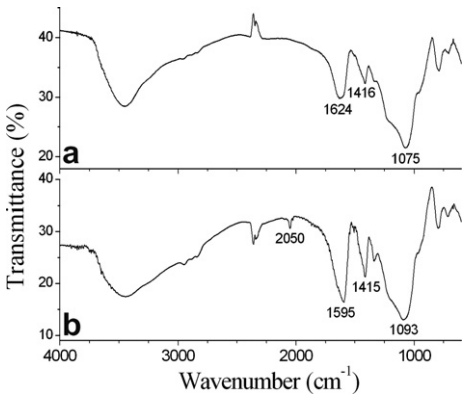

Fig. 1. IR transmission spectra of (a) a PEDTAFS sample and (b) a NiHCF–PEDTAFS sample.

BET surface area of 512 m^2/g and a BJH pore diameter of 2.2 nm, as determined by nitrogen adsorption (see Supporting Information Section). The atomic percentages of both Fe and Ni in NiHCF–PEDTAFS powder are about 5–6%, as determined by EDX spectra.

Through computer modeling, the immobilization of NiHCF onto PEDTA-functionalized surface can be summarized in the following reactions: First, a Ni(II) ion chelates with a PEDTA ligand to form a complex on the silica surface, as shown in Fig. 2a. Such a reaction is apparent when the white PEDTAFS powder turns light blue upon addition of Ni(II) solution [22]. The PM3™ method was used to model the binding of $Ni^{2+}$and TMSPEDTA. In the current modeling, a H atom (H17) was used to replace the $(CH_2)_3Si(OCH_3)_3$ group of TMSPEDTA to simplify the calculation. The model structure was referred as TMSPEDTA′. The calculated most stable structure of Ni^{2+}(TMSPEDTA′) is shown in Fig. 2a, in which the N atoms and two of the COO^- groups of TMSPEDTA′ bind Ni^{2+} to form a square planar structure. The bond lengths of Ni16–O18, Ni16–O7, Ni16–N4, Ni16–N1 are all about 1.85 Å. The other COO^- group of TMSPEDTA′ is at the axial position and the distance of Ni16–O14 is 3.69 Å. Then, ferrocyanide was immobilized on the silica surface by chelation with Ni. We modeled the structure of the complex in the initial step of the reaction between $Fe(CN)_6^{4-}$ and Ni^{2+}(TMSPEDTA′), and the calculated structure is shown in Fig. 2b. In the structure, three COO^- groups from TMSPEDTA′ and one CN^- group from $Fe(CN)_6^{4-}$ are coordinated to Ni^{2+} forming a square planar structure around Ni^{2+}ion. This suggests that when $Fe(CN)_6^{4-}$ approaches Ni^{2+}(TMSPEDTA′), the coordination around Ni^{2+} reorganizes to break two Ni–N bonds and form one COO^-–Ni and one CN^-–Ni bonds. The bond lengths of Ni13–O15, Ni13–O11, Ni13–O38, Ni13–N24 are all about 1.85 Å. The bond angle of Ni13–N24–C25 is 162° and the four atoms Ni13, N24, C25, and Fe26 are almost collinear. We postulate that the complex would continue to react with other Ni^{2+} and $Fe(CN)_6^{4-}$ to form NiHCF.

Multilayer formation of NiHCF is monitored by cyclic volatmmetry. Fig. 3a shows the cyclic voltammetric responses of a NiHCF film in 1.0 M $NaNO_3$ solution, obtained after various deposition cycles, *l*. As shown in the figure, only a single redox couple is observed in the potential range −0.3 to 1.0 V. Because Ni(II) has no electroactivity in this potential range, the redox peaks in Fig. 3a correspond to the hexacyanoferrate (II/III) redox couple. Presence of NiHCF is revealed by the characteristic half-wave potential, $E_{1/2}$, at 0.41 V [12,13]. For the first NiHCF layer, the peak current increases linearly with scan rate (υ) in the range of 10–300 mV/s, as predicted for an ideal reversible surface bound redox species. The ratio of anodic to cathodic peak currents obtained at various scan rates is almost unity, indicating stable products are formed during the redox reaction.

Peak width at half-maximum ($\Delta E_{p/2}$), which is a measure of interactions between the ions in the lattice [31]

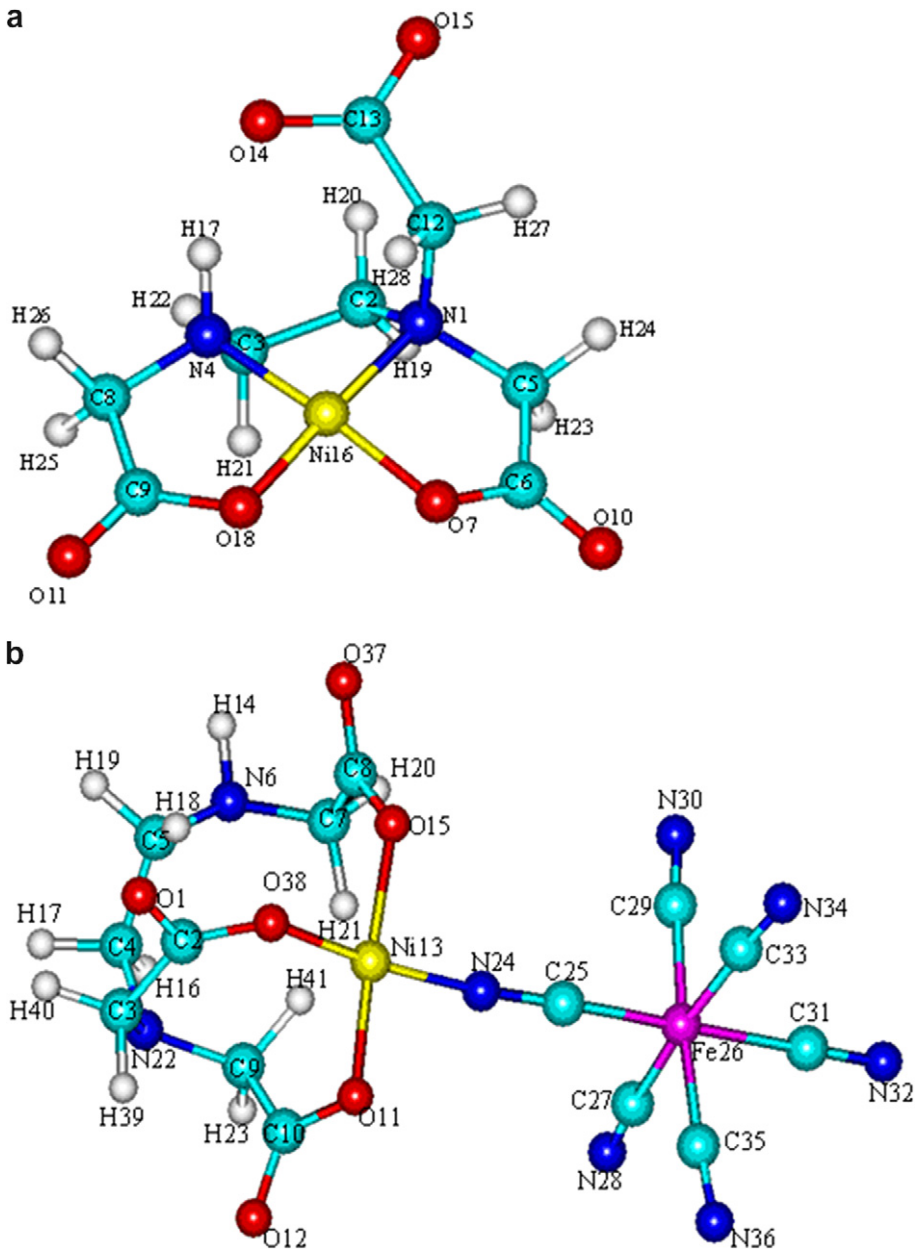

Fig. 2. Structures of (a) Ni^{2+}(TMSPEDTA′) and (b) the complex in the reaction between $Fe(CN)_6^{4-}$ and Ni^{2+}(TMSPEDTA′) through computer modeling.

and/or diffusion effect [32], is found to be 109 mV. This is broader than that expected for a thin-layer Nerstian system of 90.6/n mV [33], and broadening is known to result from repulsive site–site interactions [31] and as diffusion effect increases [32]. The peak-to-peak separation, ΔE_p, for the first layer is 59 mV at a scan rate of 100 mV/s and increases to 99 mV after 8 deposition cycles. This is larger than the theoretical prediction of zero ΔE_p for non-diffusing reversible charge transfer [34]. Similar behavior has been attributed to either slow charge-transfer kinetics within the derivatizing layer [31] or uncompensated resistance within the film [35]. The possibility of slow charge-transfer kinetics is tested by plotting ΔE_p versus $\log(\upsilon)$ [36]. The linearity of the plot indicates that slow charge-transfer kinetics is a source for peak separation. The possibility of uncompensated resistance within the film is also tested by plotting E_{pc} versus I_{pc}. The linearity of the plot indicates that the resistance effect is also a source for peak separation.

NiHCF is an analogue of the classic mixed-valence complex Prussian blue and has the same cubic framework structure in which metal atoms are linked by cyanide units [37]. The literature of bulk NiHCF suggests that stoichiometry is closely linked to structure [11,28]. Specifically, the structures typically associated with NiHCF are structural analogues of "insoluble" Prussian blue or "soluble" Prussian blue [38]. Fig. 4a shows the XRPD pattern of NiHCF–PEDTAFS powder. The well-defined peaks seen in Fig. 4a indicate that NiHCF is crystalline. The average crystallite size

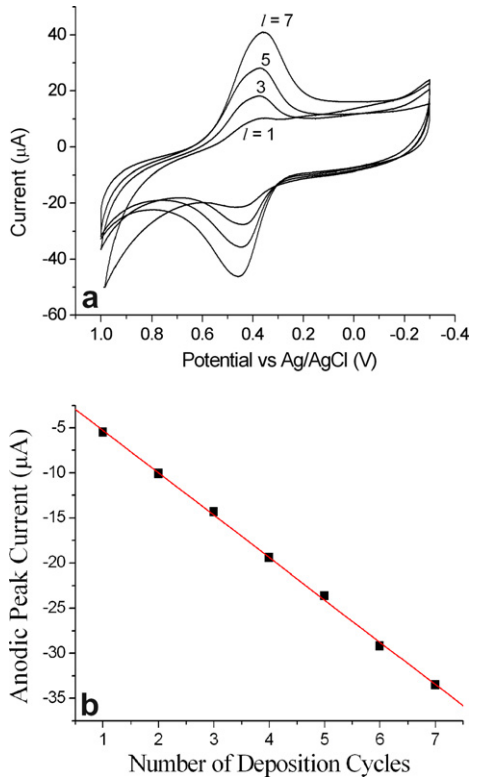

Fig. 3. (a) Cyclic voltammograms (1.0 M $NaNO_3$, scan rate 0.1 V/s) of a NiHCF film after different numbers (l) of deposition cycles. (b) A plot of the anodic current versus l.

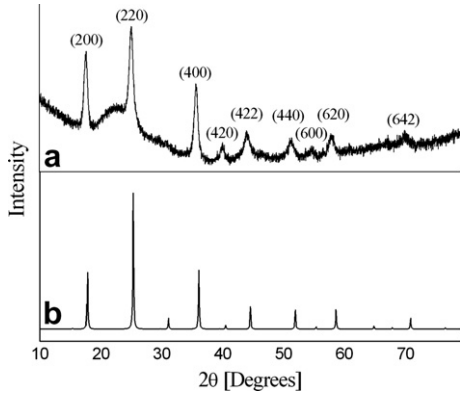

Fig. 4. (a) XPRD pattern of NiHCF–PEDTAFS. (b) Simulated XPRD pattern of reduced NiHCF ($K_2NiFe(CN)_6$, space group: F-43 m).

evaluated for the 200, 220, 400 lines by line-broadening measurements is 12.4 ± 1.5 nm. Similar average crystallite sizes have been reported for NiHCF prepared by precipitation with various $Ni^{2+}/Fe(CN)_6^{3-}$ mixing ratios [39]. Simulations of XRPD were also performed in an attempt to determine the exact structure of NiHCF prepared upon multiple sequential adsorption of Ni^{2+} and $Fe(CN)_6^{4-}$ on PEDTAFS. These XRPD simulations of reduced NiHCF ($K_2NiFe(CN)_6$) intercalated with K^+ were performed based on the single-crystal data of the "soluble" Prussian blue analogue, which crystallizes in the space group F-43 m (Fig. 4b). Comparison of the simulated and the experimental data indicates that virtually all the reflections observed in the experimental pattern exist in the simulated one. Although this class of compounds retains its cubic structure over a wide range of stoichiometries [38] and has weak peak intensities due to poor crystallinity, the condition of systematic absences as shown in Fig. 4a suggests that NiHCF prepared upon multiple sequential adsorption Ni^{2+} and $Fe(CN)_6^{4-}$ on PEDTAFS is more likely to crystallize in a face-centered space group, F-43 m, as shown in Fig. 5a. In this NaCl-type structure, iron and nickel atoms are located at $(0,0,0)$ and $(0.5,0,0)$ sites, respectively, of the cubic unit cell with the cell parameter of 0.996 nm as shown in Fig. 5a. Hence, it is expected that the NiHCF film grew via multiple sequential adsorption to form a closed-packed structure, as shown in Fig. 5b. With this assumption, the expected surface coverage of iron atoms per deposition cycle is 3.87×10^{-10} mol/cm^2.

Fig. 3b depicts the anodic peak current as a function of number of deposition cycle. It is evident from the figure that the anodic peak current increases linearly with the

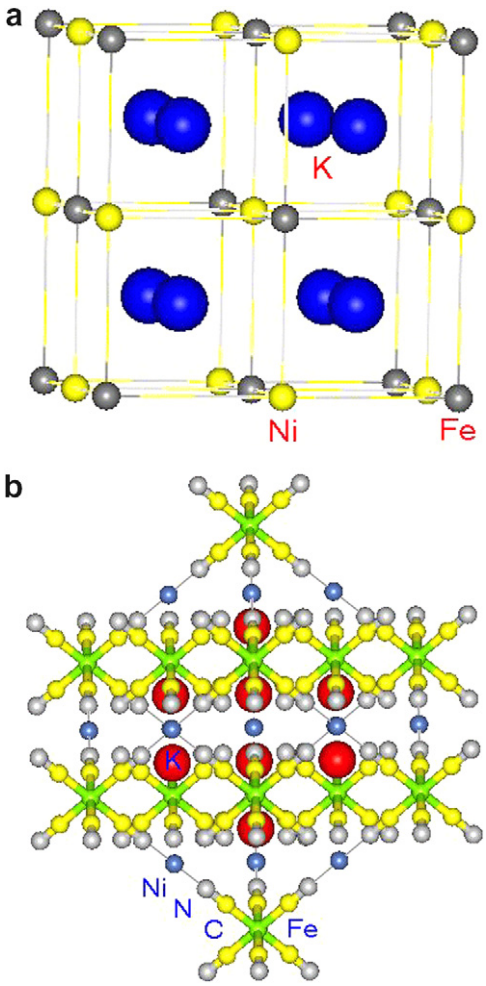

Fig. 5. (a) Unit cell of reduced NiHCF ($K_2NiFe(CN)_6$, space group: F-43 m). (b) Side view of reduced NiHCF ($K_2NiFe(CN)_6$, space group: F-43 m). Both structures are based on the single-crystal data obtained from the database.

number of deposition cycles (correlation coefficient, $r = -0.9996$), suggesting that each deposition cycle introduces a NiHCF layer. According to the simulated XRPD data, the thickness of a NiHCF layer introduced by each cycle is 0.575 nm. The surface coverage of iron atoms per deposition cycle, Γ, is given by

$$\Gamma = Q/nFA, \quad (1)$$

where Q is the amount of Coulombs obtained from integrating the anodic peak under background correction, n is the stoichiometric number of electrons involved in an electrode reaction, F is the Faraday constant, and A is the area of an electrode. The estimated surface coverage of 6.0×10^{-10} mol/cm^2 per deposition cycle is in reasonable agreement with the surface coverage expected for a monolayer of NiHCF, if a surface roughness factor of about 1.6 is assumed.

Control experiments on a TMOS-modified GC electrode or a bare GC electrode show that the NiHCF films thus formed were not robust. Repeated rinsing of such electrodes with water would cause complete loss of redox activity. On the other hand, immobilization of NiHCF on PEDTA-functionalized surface is very stable. The stability of such a modified electrode was studied by exposing it to air or storing in a buffer solution for a period of time, then recording the cyclic voltammograms. Results indicate that no loss of redox activity after storing in air or buffer. In addition, the reproducibility of the modified electrode was also examined by repetitive scans in a buffer solution. No significant change in peak currents and separation of cyclic voltammetric peaks were observed after 100 cycles of repetitive scanning (the maximum number of cycles tested).

Previous studies have shown that the redox potential of the surface-confined film varies with the alkali–metal cation present in the solution [5,7]. This has been attributed to the size dependency of cation insertion into the NiHCF lattice [37]. As such, the suitability of NiHCF-modified electrodes as cesium selective electrodes has been well-documented due to their great selectivity [5]. Similar ion-sieving behavior of NiHCF films have also been examined by other means [30,40]. The selective adsorption of Cs^+ by NiHCF in the presence of Rb^+ and other radionuclides [5,6,8] is particularly attractive for environmental monitoring of radioactive wastes. Fig. 6a shows that the responses of our NiHCF-modified electrode employed in a 1.0 M $NaNO_3$ solution or a solution of 0.01 M $CsNO_3$ and 1.0 M $NaNO_3$. As can be seen in the figure, presence of Cs^+ causes a positive shift in the peak potentials. In addition, the area under the cyclic voltammetric curve decreases and the cyclic voltammetric wave shape is broadened when compared to the sodium case. This change is reversible. Similar phenomenon had also been observed and was suggested to be due to partial deactivation of the electroactive surface species [4]. Responses of the electrode to different Cs^+ concentrations have also been studied. Results show that the redox potential shifts anodically with increasing Cs^+ concentration. As

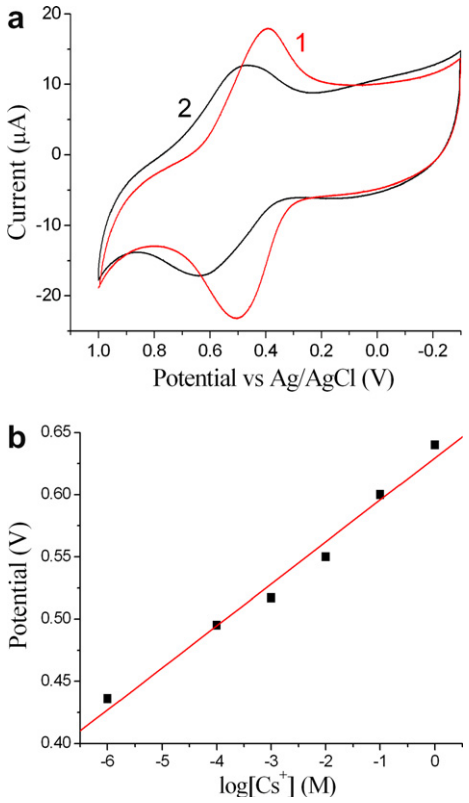

Fig. 6. (a) Cyclic voltammograms of a NiHCF film employed in (1) 1.0 M $NaNO_3$ and (2) 0.01 M $CsNO_3$ and 1.0 M $NaNO_3$. (b) A plot of $E_{1/2}$ versus log[Cs^+] for a NiHCF film employed in a 1.0 M $NaNO_3$ solution. The same electrode was used for all scans at 0.1 V/s.

shown in Fig. 6b, the Nernst plot has a linear range ($r = 0.9911$) between 10^{-6} and 1 M (supporting electrolyte = 1.0 M $NaNO_3$) and a slope of 31 ± 2 mV/decade. This slope is different from a previously reported value of 56.6 mV/decade [5], but the disagreement could arise from the structural difference between the NiHCF films. Our slope implies that two Cs^+ ions leave a NiHCF unit cell during oxidation and intercalate in the unit cell during re-reduction, since each unit cell involves 4 electrons during the redox reaction. Although partitioning of Cs^+ into NiHCF matrixes is more favorable than that of Na^+, such a phenomenon of non-exclusive Cs^+ partitioning into NiHCF had also been observed by others and was attributed to the strong repulsive Cs^+–Cs^+ interactions in NiHCF [41]. The ability to regenerate a sensor is an important issue for practical use. The high selectivity of NiHCF for Cs^+ may lead to difficulty in regeneration of the sensor. Fortunately, an electrically switched ion exchange technology has been developed to elute Cs^+ from NiHCF films [10].

3.2. Sorption of cesium

In solutions of cesium nitrate, the sorption of cesium by NiHCF was determined by batch contact experiments. Its selectivity for cesium can be inferred from its distribution coefficient (K_d) for cesium. K_d is a measure of the affinity

of an ion exchanger for a particular ion and an indicator of the selectivity of the ion exchanger to the particular ion in the presence of a complex interfering ions [17], as determined at equilibrium by the equation

$$K_d = [(C_0 - C_f)/C_f] \times (V/M) \quad (2)$$

where C_0 is the initial concentration of Cs (mg/L), C_f is the equilibrium concentration of Cs (mg/L), V is the volume of the testing solution (mL), and M is the amount of NiHCF–PEDTAFS powder or PEDTAFS powder (g). It is well-known that alkaline cations intercalate into the interstitial sites of NiHCF in order to balance the net negative charge on the matrix [37]. The sequence of affinity of NiHCF for these ions is as follows: $Na \ll K < Cs$ [7,37]. Hence, the selectivity of NiHCF–PEDTAFS for binding of cesium was evaluated at various concentrations of sodium and potassium. It should be noted that the silica matrix also adsorb alkaline cations in a relatively non-selective manner. Results from Table 1 show that NiHCF–PEDTAFS has very high selectivity for Cs even at high concentration of sodium and potassium. In all tests, over 99% Cs was removed in a single treatment. The residual concentration of cesium is below the detection limit of our AES. The distribution coefficients for cesium were found to be in excess of 1 860 000 mL/g, which are significantly higher than those of NiHCF-loaded chabazites prepared by successive impregnation with $Ni(NO_3)_2$ and $K_4Fe(CN)_6$ ($K_d = \sim 10^4$ mL/g) [8].

Since the silica matrix also adsorbs cesium, the amount of Cs sorbed by NiHCF alone was background corrected by subtracting the Cs loading on PEDTAFS powder at the same initial Cs concentration. The equilibrium cesium loading on NiHCF depends on the cesium concentration in the liquid phase, as shown in Line 1 of Fig. 7. The ion exchange equilibrium can be described by the following equation:

$$Na^+ - NiHCF + Cs^+ = Cs^+ - NiHCF + Na^+$$

with the Langmuir adsorption constant, K_{eq}, in L/mg expresses as

$$K_{eq} = (x \cdot S)/\{(S_{max} - S) \cdot S_f\}, \quad (3)$$

where C_f is the equilibrium concentration of Cs (mg/L), x is the equilibrium concentration of Na^+, S is the amount of Cs sorbed by NiHCF (mg/g), and S_{max} is the maximum amount of Cs (mg/g) that can be sorbed by NiHCF. Since the cesium binding experiments were performed in the presence of a large excess of sodium (1 M), x has little change from the initial concentration and is roughly equal to 1. Thus,

$$C_f/S = 1/(K_{eq} \cdot S_{max}) + C_f/S_{max}. \quad (4)$$

Fitting by the least squares method, as shown in Line 2 of Fig. 7, yielded values for K_{eq} of 0.011 L/mg and for S_{max} of 225 mg/g. The maximum loading of 225 mg/g is even higher than that of a Cs sorbent material derived from MCM-41 [17], which in contrast, has a surface area about two times the surface area of our material. Although the surface area of MCM-41 is higher than our material, to anchor a MHCF monolayer on its pore surface requires tedious post-functionalization steps to modify the calcined mesoporous silica. On the contrary, our mesoporous PEDTAFS is prepared by a single-step approach. Hence, steps such as calcination and post-functionalization are not needed. Moreover, it should be noted that if the sorption of Cs by the silica matrix is also taken into account, the Cs loading of NiHCF–PEDTAFS can be as high as 309 mg/g at an initial Cs concentration of 616 ppm. Such a high Cs loading capacity is a combined result of the porous nature of the sol–gel material and multilayer character of the NiHCF film.

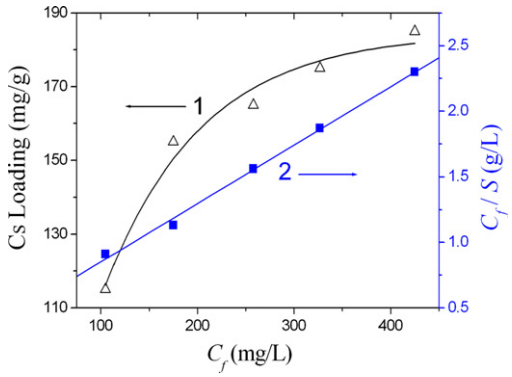

Fig. 7. (1) Langmuir sorption isotherm of Cs^+ in NiHCF and (2) its linear fitting after the transformation by the Langmuir Eq. (4).

Table 1
Cs binding in the presence of competition cations[a]

Sample	C_0 (ppm)	C_f (ppm)	K_d (mL/g)
3.0 M KNO_3	104	<0.1	>1 880 000
3.0 M $NaNO_3$	109	<0.1	>1 980 000
0.01 M $NaNO_3$	104	<0.1	>1 880 000
0.01 M KNO_3	105	<0.1	>1 900 000
1.0 M $NaNO_3$ + 1.0 M KNO_3	103	<0.1	>1 860 000

[a] 100 ml solutions, 0.05 g NiHCF–PEDTAFS.

4. Conclusion

We have demonstrated the feasibility of building a NiHCF multilayer with a controlled thickness on a porous functionalized sol–gel material through multiple sequential adsorption. This approach is very simple and may be extendable to other MHCFs. Such a composite has been used as a cesium sensor with a sensitivity down to 10^{-6} M and as a selective cesium sorbent with a maximum loading of at least 225 mg/g. The unique combination of the porous nature of sol–gel materials and multilayer character of the NiHCF film makes the composite a strong candidate for cleanup of cesium-containing nuclear wastes and contaminated groundwater.

Acknowledgments

We gratefully acknowledge support of this work by the National Science Council (ROC) Grant Numbers NSC 91-2815-C-194-022-M and NSC 93-2113-M-194-016.

Appendix A. Supplementary data

Supplementary data associated with this article can be found, in the online version, at doi:10.1016/j.micromeso.2007.05.057.

References

[1] C.J. Northrup, L.J. Jardine, M.J. Steindler, IAEA-SM-261/31, International Atomic Energy Agency, Vienna, 1983.
[2] P.A. Haas, Sep. Sci. Technol. 28 (1993) 2479.
[3] M.A. Lilga, R.J. Orth, J.P.H. Sukamto, S.M. Haight, D.T. Schwartz, Sep. Purif. Technol. 11 (1997) 147–158.
[4] L.J. Amos, A. Duggal, E.J. Mirsky, P. Ragonesi, A.B. Bocarsly, P.A. Fitzgerald-Bocarsly, Anal. Chem. 60 (1988) 245.
[5] H. Dussel, A. Dostal, F. Scholz, Fresenius J. Anal. Chem. 355 (1996) 21.
[6] S. Kawamura, S. Shibata, K. Kurotaki, Anal. Chim. Acta 81 (1976) 91.
[7] S. Sinha, B.D. Humphrey, A.B. Bocarsly, Inorg. Chem. 23 (1984) 203.
[8] H. Mimura, M. Kimura, K. Akiba, Y. Onodera, Sep. Sci. Technol. 34 (1999) 17.
[9] I.M. Ismail, M.R. El-Sourougy, N.A. Moneim, H.F. Aly, J. Radioanal. Nucl. Chem. 240 (1999) 59.
[10] M.A. Lilga, R.J. Orth, J.P.H. Sukamto, S.D. Rassat, J.D. Genders, R. Gopal, Sep. Purif. Technol. 24 (2001) 451.
[11] C. Loos-Neskovic, M. Fedoroff, E. Garnier, P. Gravereau, Talanta 31 (1984) 1133.
[12] A.B. Bocarsly, S. Sinha, J. Electroanal. Chem. 137 (1982) 157.
[13] X. Zhou, S. Wang, Z. Wang, M. Jiang, Fresenius J. Anal. Chem. 345 (1993) 424.
[14] C.-X. Cai, H.-X. Ju, H.-Y. Chen, Anal. Chim. Acta 310 (1995) 145.
[15] S. Bharathi, V. Yegnaraman, G.P. Rao, Langmuir 11 (1995) 666.
[16] Y. Guo, A.R. Guadalupe, O. Resto, L.F. Fonseca, S.Z. Weisz, Chem. Mater. 11 (1999) 135.
[17] Y. Lin, G.-E. Frexell, H. Wu, M. Engelhard, Environ. Sci. Technol. 35 (2001) 3962.
[18] C. Liu, Y. Huang, N. Naismith, J. Economy, J. Talbott, Environ. Sci. Technol. 37 (2003) 4261.
[19] R.C. Millward, C.E. Madden, I. Sutherland, R.J. Mortimer, S. Fletcher, F. Marken, Chem. Commun. (2001) 1994.
[20] M. Pyrasch, B. Tieke, Langmuir 17 (2001) 7706.
[21] S. Bharathi, M. Nogami, S. Ikeda, Langmuir 17 (2001) 7468.
[22] P. Tien, L.-K. Chau, Chem. Mater. 11 (1999) 2141.
[23] HyperChem pro 7.0, Hypercube Inc., Gainesville, FL, USA, 2002.
[24] C. Ohe, H. Ando, Y. Urai, M. Yamamoto, K. Itoh, J. Phys. Chem. B 103 (1999) 435.
[25] J.E. Tackett, Appl. Spectrosc. 43 (1989) 483.
[26] Y.-T. Tao, J. Am. Chem. Soc. 115 (1993) 4350.
[27] A. Gericke, H. Huhnerfuss, Thin Solid Films 245 (1994) 74.
[28] C. Loos-Neskovic, M. Fedoroff, E. Garnier, Talanta 36 (1989) 749.
[29] S.M. Haight, D.T. Schwartz, M.A. Lilga, J. Electrochem. Soc. 146 (1999) 1866.
[30] M. Pyrasch, A. Toutianousch, W. Jin, J. Schnepf, B. Tieke, Chem. Mater. 15 (2003) 245.
[31] P.J. Peerce, A.J. Bard, J. Electroanal. Chem. 114 (1980) 89.
[32] K. Aoki, K. Tokuda, H. Matsuda, J. Electroanal. Chem. 146 (1983) 417.
[33] E. Laviron, L. Roullier, C. Degrand, J. Electroanal. Chem. 112 (1980) 11.
[34] E. Laviron, J. Electroanal. Chem. 101 (1979) 19.
[35] P. Daum, R.W. Murray, J. Phys. Chem. 85 (1981) 389.
[36] R.S. Nicholson, Anal. Chem. 37 (1965) 1351.
[37] L.F. Schneemeyer, S.E. Spengler, D.W. Murphy, Inorg. Chem. 24 (1985) 3044.
[38] W.A. Steen, S.-W. Han, Q. Yu, R.A. Gordon, J.O. Cross, E.A. Stern, G.T. Seidler, K.M. Jeerage, D.T. Schwartz, Langmuir 18 (2002) 7714.
[39] S. Yamada, K. Kuwabara, K. Koumoto, Mater. Sci. Eng. B 49 (1997) 89.
[40] W. Jin, A. Toutianoush, M. Pyrasch, J. Schnept, H. Gottschalk, W. Rammensee, B. Tieke, J. Phys. Chem. B 107 (2003) 12062.
[41] K.M. Jeerage, W.A. Steen, D.T. Schwartz, Chem. Mater. 14 (2002) 530.